SIMULATION OF TURBOFAN ENGINE FLOW SUPPRESSION EFFECTS

M. Berens, M. de Rosa Jacinto da Silva, B. Gerl
Technische Universität Wien, Research Group Aircraft Systems E307-02-2, Lehárgasse 6, 1060 Vienna, Austria

ABSTRACT

When turbofan engines are installed under the wing, the static pressures at the engine nozzles are often locally higher than those of the undisturbed environment. An increased static pressure downstream of an unchoked propelling nozzle leads to a reduction in nozzle pressure ratio, nozzle mass flow rate and gross thrust – referred to as flow suppression. The conventional industry turbofan thrust accounting method for flight and wind tunnel testing is based on a mass flow and momentum consideration and does not take the local static pressure at the nozzle of the installed engine into account. Neglecting flow suppression, the determined thrust is often overestimated. While this thrust accounting simplification was permissible for previous engine generations, the mass flow rate and thrust bias increases significantly for designs with increasing bypass and decreasing fan pressure ratios. Aerodynamic data is corrected for nacelle external flow induced suppression effects dominating in high speed conditions according to standard industry practice but no such corrections are applied to wing induced flow suppression effects which dominate in low speed conditions. NASA's Common Research Model (CRM) configuration has been used for a parametric study based on full configuration Reynolds Averaged Navier-Stokes (RANS) computations complemented by rapid CFD results for the low speed high-lift flap effects. The impact of the nozzle back-pressure effect on the determination of mass flow rates and thrusts depending on aircraft layout, engine/nacelle design features, high-lift configuration, operational and flight condition parameters is explained. A straight forward data reduction approach avoiding systematic bias errors due to nozzle backpressure effects based on the continuity equation is proposed. Difficulties in measuring static pressures at the nozzle exit station are avoided by moving the mass flow evaluation station forward into the duct where measurements of representative static pressures are more robust. The suggested approach can not only be employed for wind tunnel tests utilizing Turbofan Propulsion Simulators (TPS) and Through Flow Nacelles (TFN) but also for full scale in-flight thrust determination.

Keywords: Flow Suppression, Turbofan, CFD, Thrust Drag Bookkeeping, CRM, TPS, TFN

NOMENCLATURE

Latin Symbols

A	Cross section area	m²
c_D	Discharge coefficient	-
c_L	Lift coefficient	-
cp	Pressure coefficient	-
F_G	Gross thrust	N
F_E	Ram drag	N
F_N	Net thrust	N
$FNPR$	Fan nozzle pressure ratio = PT_{19} / P_{100}	-
FPR	Fan total pressure ratio	-
M	Mach number	-
$\dot{m}$	Mass flow rate	kg/s
$\dot{m}^*$	Mass flow function	-
q_0	Freestream dynamic pressure= $\frac{1}{2} \cdot \gamma \cdot P_0 \cdot M_0^2$	N/m²
$q_{kin,noz}$	TFN kinetic pressure = $P_{T,0} - P_{noz}$	N/m²
P	Static pressure	N/m²
$PR = P_T/P$	Total to static pressure ratio	-
$PR19$	Fan nozzle pressure ration PT_{19} / P_{19}	-
P_T	Total pressure	N/m²
T_T	Total temperature	K
R	Ideal gas constant = 287.05	J/(kg·K)
Re_c	Chord based Reynolds number	-
V	Jet velocity	m/s

Greek Symbols

α	Angle of attack	deg
β	Sideslip angle	deg
δ_{flap}	Flap deflection angle	deg

doi: 10.25967/570424

γ	Ratio of specific heats for air = 1.4	-
ζ	Pressure loss coefficient w. r. t. $q_{kin,19}$	-

Indices

0	Freestream
00	Core jet downstream nozzle
1	Intake highlight station
5	Core duct downstream turbine
15	Bypass duct downstr. fan stage
9	Core nozzle exit
19	Fan nozzle exit
100	Fan jet downstream nozzle
actual	Actual value
crit	Critical conditions (M_{local} = *1*)
eff	Effective
FNPR	Referring to FNPR
i	inner
NEF	Nacelle external flow induced nozzle pressure
noz	nozzle
PR19	Referring to PR19
o	outer
SAE	Society of Automotive Engineers [3]
WIN	Wing induced nozzle pressure

1. INTRODUCTION TO ENGINE FLOW SUPPRESSION EFFECTS

First of all, one needs to distinguish between the physical effects of flow suppression on the one hand and thrust determination bias errors on the other hand. Focus in the present paper will be laid on the latter.

In-flight turbofan engine and wind tunnel Turbofan Propulsion Simulator (TPS) thrust is determined based on gas path measurements of total pressure, total temperature and static pressure as well as duct respectively nozzle cross section areas. Because of pressure losses between the measurement (inside the duct) and the accounting stations (usually the nozzle exit), engines and TPS are mass flow rate and thrust calibrated in engine calibration facilities (ECFs). The mass flow rates are determined by accurate reference mass flow meters and reference thrust is measured with balances. Deliverables of the calibration runs are discharge and thrust coefficients which can subsequently be used to correct wind tunnel or in-flight gas path measurements derived ideal mass flow and thrust data. Because of no external nacelle flow, operating engines and TPS in ECFs are somehow ideal and it is assumed that the flow suppression is zero.

External nacelle flow alone will already change the static pressure at the nozzle. When installed on a wing, the airframe will induce additional pressures at the nozzle station.

De Wolf [1] highlighted that the simplified thrust determination approach based on the assumption of the freestream static pressure at the fan nozzle exit station used for high bypass ratio TPS may produce bias errors for future fan stage designs with decreased fan pressure ratios. The effects of flow suppression on thrust determination are also addressed in [2] and more details on how to cope with these effects are documented in [3].

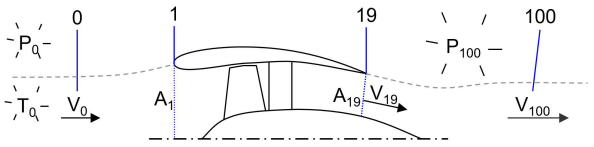

FIG 1. Bypass duct station numbering

A simple analysis is made in order to illustrate the fundamental effects. This analysis is based on following assumptions

- Single duct
- Convergent nozzle
- Free-stream = thrust direction
- Ideal flow, no losses
- 1D stream-tube assessment

The gross thrust is derived from the momentum equation (Newton's second law)

(1) $$F_G = \dot{m} \cdot V \quad .$$

The nozzle mass flow rate is determined from the compressible continuity equation

(2) $$\dot{m} = A \cdot \sqrt{\frac{2 \cdot \gamma}{R \cdot (\gamma - 1)}} \cdot \frac{P_T}{\sqrt{T_T}} \cdot PR^{-\frac{1}{\gamma}} \cdot \sqrt{1 - PR^{\frac{1-\gamma}{\gamma}}} \quad .$$

If the pressure ratio exceeds $PR_{crit} = \left(\frac{2}{\gamma+1}\right)^{-\frac{\gamma}{\gamma-1}}$, the local flow Mach number at the convergent nozzle exit station becomes unity. The nozzle chokes and the effective pressure ratio is limited to the critical value, hence

(3) $$\dot{m} = A \cdot \sqrt{\frac{\gamma}{R} \cdot \left(\frac{2}{(\gamma+1)}\right)^{\frac{\gamma+1}{\gamma-1}}} \cdot \frac{P_T}{\sqrt{T_T}} \quad .$$

Now, exemplarily considering the bypass (= fan) duct and referring to the station numbers shown in FIG 1, two evaluations will be compared at the nozzle exit station with

a) $PR = (P_{T,19}/P_{19}) = PR19$ and $\dot{m} = \dot{m}_{PR19}$ and

b) $PR = (P_{T,19}/P_{100}) = FNPR$ and $\dot{m} = \dot{m}_{FNPR}$.

In-flight and wind-tunnel thrust determination is based on b). Use of b) introduces a bias error in mass flow rate and on thrust whenever $P_{19} \neq P_{100}$. Note that $P_{100} = P_0$ for free flight conditions.

The local static pressure rise at the nozzle in free flight conditions can be conveniently expressed in terms of a pressure coefficient

(4) $$cp_{19} = \frac{P_{19} - P_0}{q_0} \quad .$$

With this definition, the local nozzle pressure ratio (*PR19*) and the fan nozzle pressure ratio (*FNPR*) can be related by the following equation

(5) $$\frac{FNPR}{PR19} = 1 + \frac{1}{2} \cdot cp_{19} \cdot \gamma \cdot M_0^2 \quad .$$

indicating that the offset between *FNPR* and *PR19* is both depending on cp_{19} and M_0.

The relation of both pressure ratios is shown in FIG 2 for a freestream Mach number of 0.8. In the reference case of $cp_{19} = 0$, *FNPR* = *PR19*. If the pressure coefficient at the nozzle is increased to $cp_{19} = 0.6$ and assuming that *FNPR* = PR_{crit}, the actual local pressure ratio is only *PR19* = *1.5*. When the data is evaluated according to the *FNPR* approach b) the nozzle is assumed to choke while it is physically still far from choking.

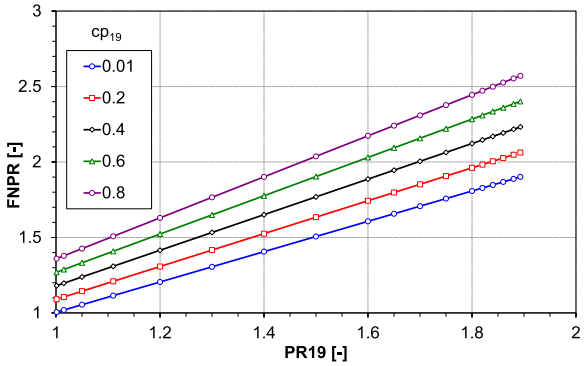

FIG 2. *FNPR* as function of *PR19* with cp_{19} as parameter for $M_0 = 0.8$

FIG 3 shows the same effect in terms of the dimensionless mass flow function:

(6) $$\dot{m}^*_{FNPR} = \frac{\dot{m}}{A_{19} \cdot \sqrt{\frac{2 \cdot \gamma}{R \cdot (\gamma - 1)}} \frac{P_{T,19}}{\sqrt{T_{T,19}}}}$$

$$= FNPR^{-\frac{1}{\gamma}} \cdot \sqrt{1 - FNPR^{\frac{1-\gamma}{\gamma}}} \quad .$$

When the local nozzle pressure ratio *PR19* equals the critical pressure ratio, the nozzle is physically choked and the mass flow function is at its maximum value. In case of no flow suppression, i.e. $cp_{19} = 0$, the *PR19* as well as the *FNPR* based dimensionless mass flow function decreases. If the local nozzle static pressure is higher than the freestream static pressure, *FNPR* is higher than *PR19*.

Taking the previous example of $cp_{19} = 0.6$ and performing the mass flow function evaluation based on *FNPR*, the nozzle is assumed choked down to an actual local *PR19* of *1.5*. Furthermore, the diagram (FIG 3) illustrates that the lower *PR19*, the greater the spread of the curves between different cp_{19}'s. Apparently, the mass flow rate bias errors increase with decreasing nozzle pressure ratios.

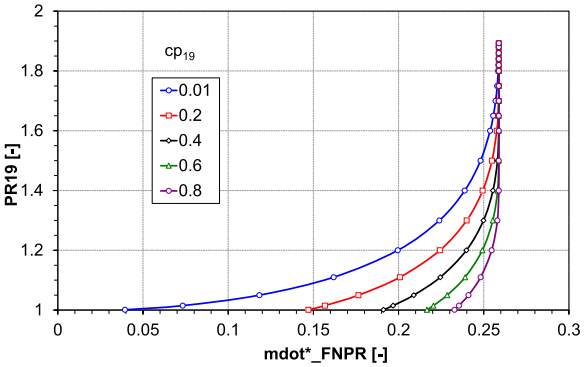

FIG 3. *PR19* vs mass flow function with cp_{19} as parameter for $M_0 = 0.8$

2. SUPPRESSION EFFECTS ANALYSIS

2.1. Computational Model

The present chapter quantifies the pressure rise at wing mounted turbofan engine nozzles utilizing NASA's Common Research Model (CRM), that represents a contemporary long-range transonic transport aircraft [4]. The CRM was developed to provide a platform for open research and particularly for CFD validation. The geometry is openly available as well as wind tunnel test results obtained with the original 0.027 scale high-speed model (HS-CRM) in the course of tests in NASA's National Transonic Facility (NTF) and later in the European Transonic Windtunnel (ETW) [5] covering a range of various Reynolds- and Mach number combinations.

A slightly modified CRM low-speed model (LS-CRM) was developed at a later point in time [6].

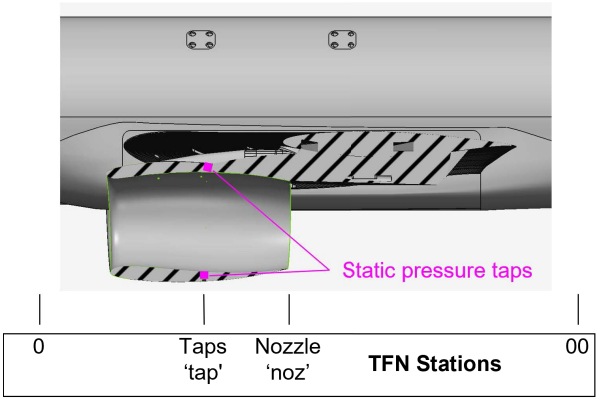

FIG 4. NASA HS-CRM cut through TFN and station designations

The port Through Flow Nacelle (TFN) of the HS-CRM is equipped with six circumferentially distributed internal wall static pressure taps at the station shown in FIG 4 which will be used to validate the numerical model results.

An objective was to study following effects in low-speed (LS) as well as high-speed (HS) flight conditions

- Mach number (LS and HS)
- Angle of attack (LS and HS)
- High-lift system (LS)
- Sideslip (LS and HS)
- TFN Nozzle configuration (HS).

Since the airframe induced pressures can be regarded as first order effects and because transonic effects do not fundamentally change the effects at some distance from the wing, a numerically efficient Vortex Lattice Method (VLM) computation was employed for a first study [7]. The VLM++ code used for this is described in [8].

In order to improve the simulation fidelity, the VLM++ parametric study was partially repeated in a second study using the commercial RANS solver Siemens StarCCM+ of which results are presented in the present paper.

StarCCM+ uses a finite volume method using an implicit coupled energy solver with a 2nd order discretization and a Roe flux-difference splitting scheme.

The turbulence model was k-ω Menter-SST with a 1st order convection scheme and linear constitutive relation. The discretization was optimized to ensure Y+ values lower than 3 (FIG 5).

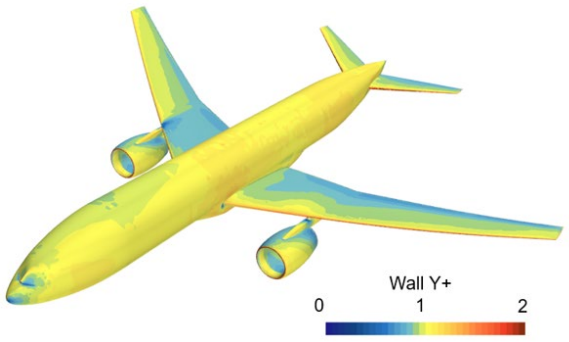

FIG 5. NASA HS-CRM: Surface contours of Y+

Simulation cases are described by following settings

- Re_c = 5x10^6
- M_0 = 0.2 and 0.7
- α = 3.0° (baseline) + var.
- β = 0° (baseline) + var.
- $\delta_{flap,i} = \delta_{flap,o}$ = 0°

For studying of high-lift configuration effects only the trailing edge flap was tentatively modelled with a simple hinged flap model according to the "Simplified High Lift CRM configuration" of [9]. Since RANS computations were only conducted with the clean configuration HS-CRM model, flap effects were taken from the first VLM-based study [7]. FIG 6 depicts the VLM flap configuration with inner and outer flap deflections. VLM does not explicitly model fluid dynamic phenomena like boundary layer separation and this is why circulation and lift are often overpredicted. Note that the effective flap angle $\delta_{flap,eff}$ for the VLM computation was halved as a consequence compared to the geometrical angle δ_{flap} based on recommendations of Torenbeek [10].

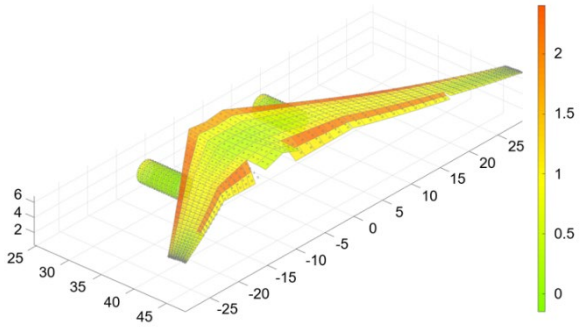

FIG 6. Trailing edge flap modeled with VLM++ (α = 3.0°, β = 0.0°, M_0 = 0.2, $\delta_{flap,i} = \delta_{flap,o}$ = 50°)

2.2. Comparison of CFD with Wind Tunnel Data

FIG 7 shows the c_L versus α plot comparison of the RANS with the selected NTF wind tunnel test polar. The fit in the "linear" region of the polar is fair. CFD and wind tunnel results diverge for angles of attack greater than 6.5 deg, though. A x-z-cut through nacelle and wing depicting the pressure coefficients is shown in FIG 10 a) while the exit plane averaged *cp's* at the nozzle exit station are shown in FIG 8. FIG 9 compares measured and computed nacelle internal pressures. The shapes of the curves are similar but the numerical cp's are roughly 0.08 higher than those measured in the NTF wind tunnel test. This difference cannot be explained by the slightly different data reduction approaches (StarCCM+: wall line averaged, Wind Tunnel Test: taps averaged).

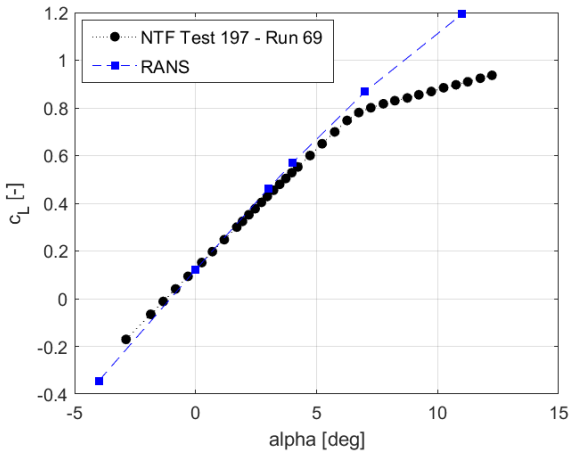

FIG 7. HS-CRM lift curve: Comparison of StarCCM+ polar with wind tunnel test data (α = Var., β = 0.0°, M_0 = 0.7, $\delta_{flap,i} = \delta_{flap,o}$ = 0°)

A TFN loss coefficient of $\zeta = 0.05$ referring to the nozzle kinetic pressure $q_{kin,noz}$ reproduces the RANS nacelle internal pressures in a simplified 1-D TFN model as described in [7]. This is only half the value used previously

to match the NTF wind tunnel results.

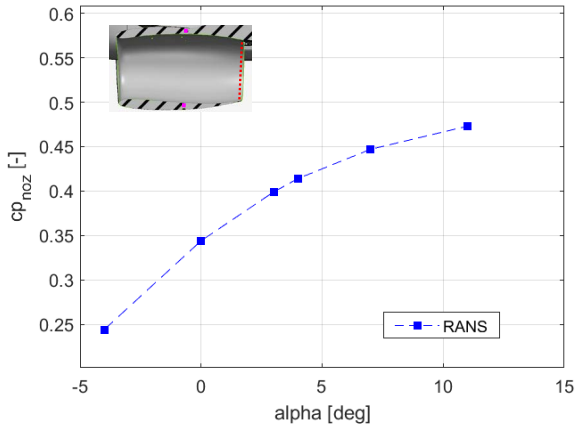

FIG 8. HS-CRM TFN nozzle exit plane averaged pressure coefficients

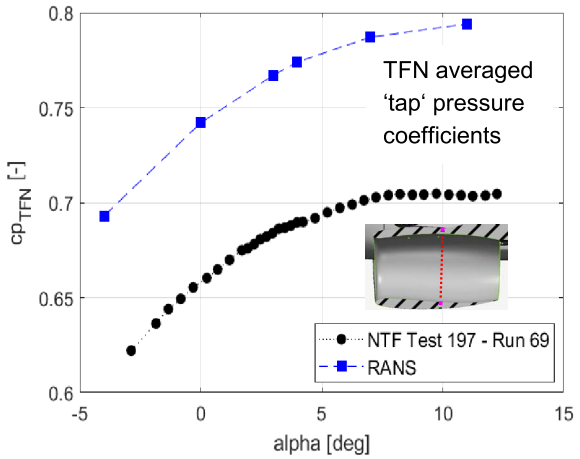

FIG 9. HS-CRM TFN internal 'tap' pressure coefficients: Comparison of StarCCM+ (wall line averaged) with wind tunnel test data (taps averaged)

2.3. Parametric Study

A numerical parametric study was conducted by varying configuration and flight condition parameters to identify the sensitivity of the wing induced nozzle pressures.

The results of the study are summarized in TAB 1. Minimum and maximum bounds have been selected based on following criteria:

a) Aircraft operational relevance
b) Computed data points preferred over interpolation
c) Credibility of data point numerical solution

A tentative ranking of nozzle cp-effects puts the flap deflection angle at the first position followed by the angle of attack, the freestream Mach number and the TFN nozzle configuration/geometry. Given the limited range of sideslip angles from -10° to 0°, the influence of this parameter is smallest.

It has been pointed out in [3] that the nozzle geometries have a significant influence on the nozzle pressures and this is corroborated by the significant reduction of the fan nozzle pressure coefficient in case of adding an annular body that represents the core of a turbofan engine as shown in FIG 10 b) as compared to the original HS-CRM TFN configuration FIG 10 a).

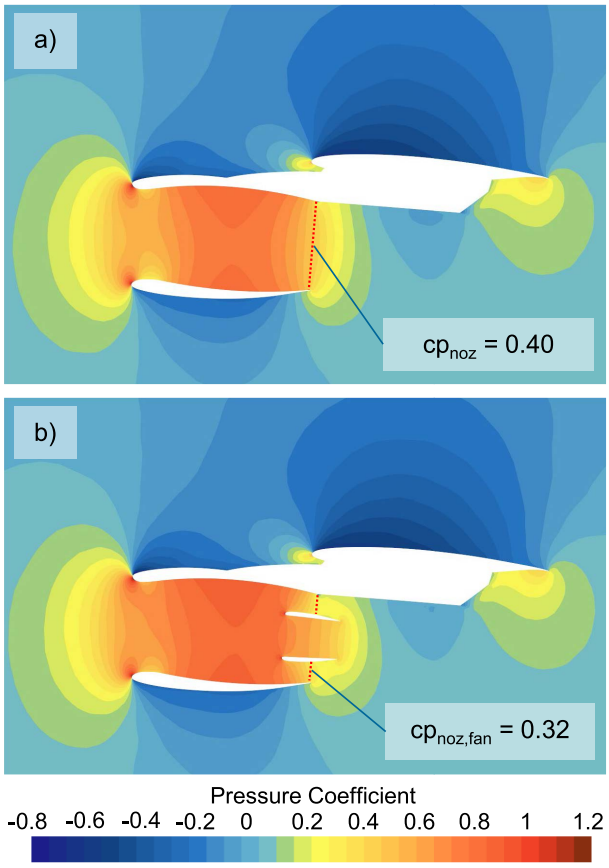

FIG 10. Effect of TFN core representation on nozzle pressure coefficient. a) Reference HS-CRM TFN b) Configuration with core representation (α = 3°, β = 0.0°, M_0 = 0.7, $\delta_{flap,i} = \delta_{flap,o}$ = 0°)

Blockage of the nozzle flow by the additional core body reduces the mass flow rate through the TFN and the nacelle internal pressure increases. This blockage is only partially compensated by the reduced fan nozzle suppression (lower cp_{noz}'s).

3. SPLIT INTO WING INDUCED (WIN) AND EXTERNAL NACELLE FLOW (NEF) SUPPRESSION EFFECTS

The previous section discussed the principle flow suppression effects. The legacy industry practice is to correct wind tunnel and flight test engine mass flow (and hence also thrust) data for nacelle external flow (NEF) effects. The data is obtained from dedicated RANS computations of the isolated nacelles [3]. In the present discussion installed aircraft data with the NEF reference values subtracted will be referred to as airframe or wing induced effects (WIN).

TAB 1. Summary of parametric study (Re_c = $5x10^6$). Notes: $\delta_{flap} = \delta_{flap,i} = \delta_{flap,o}$. TFN nozzle configuration: cp_{noz}'s apply for single stream (Ref.) or TFN fan nozzle with core body representation (CB).

Parameter	M_0	α	β	δ_{flap}	Noz. Conf.	min	max	span	$cp_{noz,min}$	$cp_{noz,max}$	Δcp_{noz}	Data source
Mach Number	Var.	3°	0°	0°	Ref.	0.2	0.7	0.5	0.32	0.40	0.08	RANS
Angle of Attack	0.7	Var.	0°	0°	Ref.	0°	+ 7°	7°	0.35	0.45	0.10	RANS
Sideslip angle	0.2	3°	Var.	0°	Ref.	-10°	0°	10°	0.27	0.32	0.05	RANS
Flap angle	0.2	3°	0°	Var.	Ref.	0°	50°	50°	0.40	0.54	0.14	VLM
TFN nozzle configuration	0.7	3°	0°	0°	Var.	Ref.	CB	N/A	0.40	0.32	-0.08	RANS

3.1. NASA HS-CRM Through Flow Nacelle

For the sake of a completeness, the effects of the NASA HS-CRM TFN are discussed. The nozzle exit station pressure coefficient is particularly high for this TFN design (FIG 11).

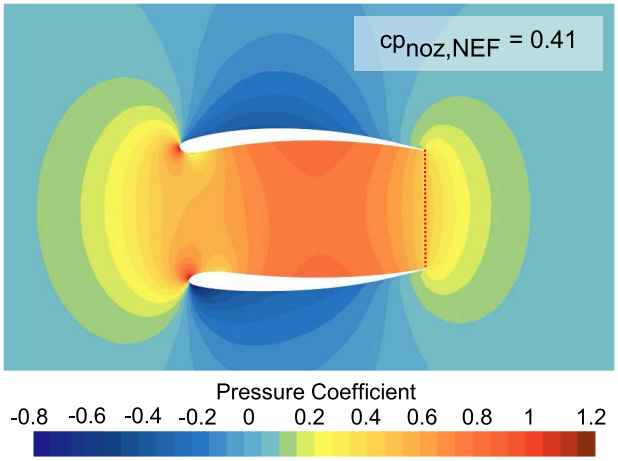

FIG 11. NEF pressure coefficients of isolated TFN nacelle (α = 0°, β = 0.0°, M_0 = 0.7)

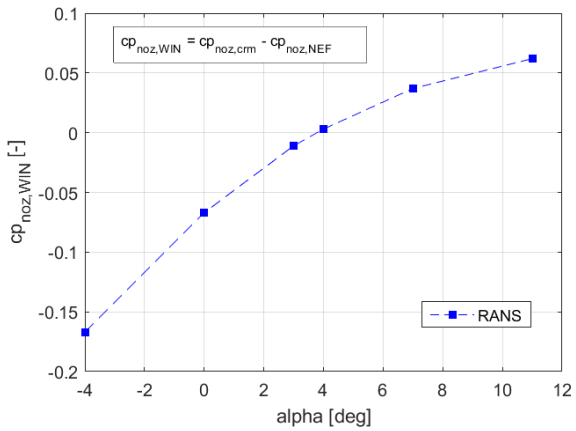

FIG 12. WIN pressure coefficients of HS-CRM installed TFN nacelle (α = *Var.*, β = *0.0°*, M_0 = *0.7*)

Subtracting the $cp_{noz,NEF}$ from the α-polar of the installed configuration for M_0 = *0.7*, the corresponding wing induced (WIN) contributions are obtained as illustrated by FIG 12.

WIN flow suppression is only observed for angles of attack greater than 4°. Below that angle, the installation influence yields less suppression compared to the isolated nacelle reference case with the consequence that mass flow rate is higher than for the isolated nacelle.

3.2. Thrust Producing Turbofan Nacelles

The present section addresses the effects of the NEF on thrust producing turbofan nacelles. The nacelle disturbs the flow in a principally similar way as any other aircraft elementary body like fuselage or wing. The engine exit stream tube of a thrust producing engine has a smaller diameter than the engine entry stream tube (note that the opposite is true for TFN's). This is mandated by continuity because the engine exit flow velocity must be higher to let the engine produce forward thrust.

The nacelle external flow effects can be characterised by imagining that the jet velocities are fixed but the nacelle external flow velocity is increasing yielding

- a reduction in the velocity difference between jets and the environment
- a reduced velocity difference and hence a reduced jet plume spreading and
- increased nozzle pressures.

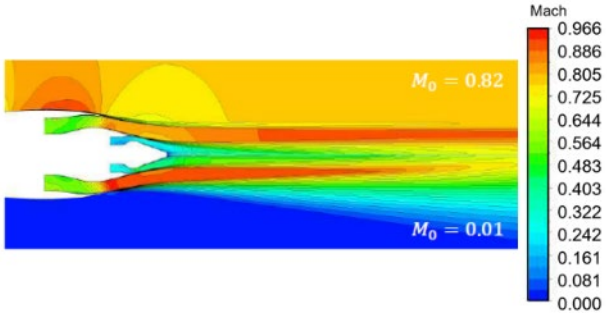

FIG 13. Mach number contour plot of TPS exhaust with and without external flow at *FNPR = 1.74*. Reproduced from Figure 5.3 [11]

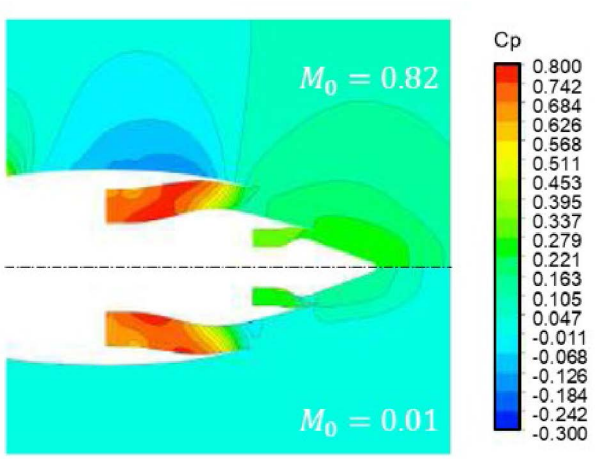

FIG 14. Pressure coefficient field of TPS exhaust with and without external flow at *FNPR = 1.74*. Reproduced from Figure 5.3 [11]

The first two effects are shown by FIG 13 and the latter effect by FIG 14 which are both reproduced from Campomanes [11].

Having simulated several *FNPR's (1.43, 1.58, 1.74)*, the influence of the engine power setting was found to be small. However, the exact pressure rise depends on the geometries of nacelle and engine core cowl and the core plug [3]. Apart from geometry, this renders the freestream Mach number as the main influencing parameter.

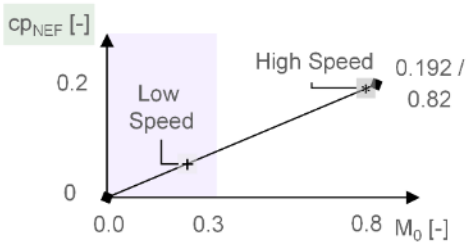

FIG 15. Nacelle external flow NEF induced fan nozzle exit pressure coefficient rise with freestream Mach number M_0 based on data for a VHBR TPS. Based on Figure 5.4 [11]

FIG 15 shows the development of the fan nozzle exit pressure coefficient with freestream Mach number for a generic Very High Bypass Ratio (VHBR) engine nacelle configuration. Between the two data points, *M0 = 0* and *M0 = 0.82*, a linear development is stipulated. The low-speed domain for Mach numbers between *0* and *0.3* is highlighted by a blueish shading.

FIG 16 from [3] presents the nacelle external flow suppression effects in terms of change in nozzle discharge coefficient depending on the actual nozzle pressure ratio. Note that the low-speed domain is again highlighted by a blueish shading.

The nozzle discharge coefficient relates the actual mass flow rate $\dot{m}_{actual}$ to an ideal mass flow rate $\dot{m}_{FNPR}$ that would be obtained if the nozzle flow were lossless

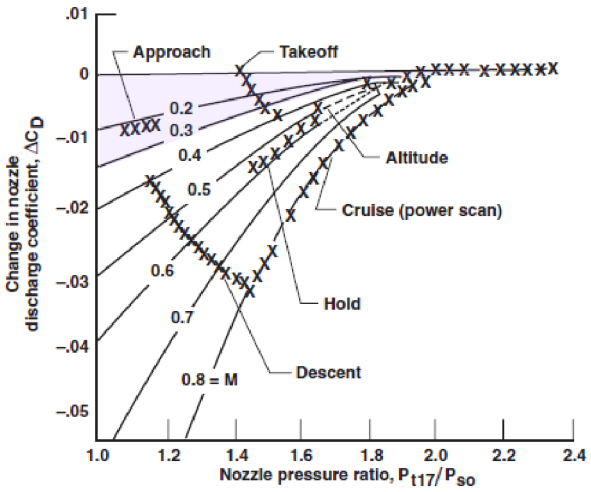

FIG 16. External flow induced change in nozzle discharge coefficient. Reproduced Figure 7.8 [3]

(7) $$c_{D,FNPR} = \frac{\dot{m}_{actual}}{\dot{m}_{FNPR}} \quad .$$

In calibration mode, $\dot{m}_{actual}$ is replaced by the reference mass flow and the discharge coefficient is determined.

Further, the bias in terms of discharge coefficient is

(8) $$\Delta c_{D,SAE} = c_{D,FNPR} \cdot \left(1 - \frac{\dot{m}_{FNPR}}{\dot{m}_{PR19}}\right) \quad .$$

Practically, changes in nozzle discharge coefficients due to NEF flow suppression are applied to the engine test bench (ECF) *c_D's* to obtain figures corresponding to conditions with external nacelle flow.

4. FAN PRESSURE RATIO INFLUENCE ON FLOW SUPPRESSION IN LOW- AND HIGH-SPEED CONDITIONS

An introduction to flow suppression effects was presented in chapter 1 with a focus laid on the primary effects of mass flow rate quantification bias. In the present chapter the scope will be extended to the directly dependent net thrust effects. Again, the bypass (= fan) duct is exemplarily chosen for the derivation but the principles are applicable for the core duct as well.

The fan pressure ratio is defined as the ratio of the fan nozzle exit total pressure to the freestream total pressure (refer to FIG 1 for station number indices)

(9) $$FPR = \frac{P_{T,19}}{P_{T,0}} \quad .$$

The freestream total pressure in turn is obtained from the freestream static pressure and the freestream Mach number

TAB 2. Data for low speed take-off and high-speed cruise cases.

Case		M_0 [-]	α [°]	δ_{flaps} [°]	c_L [-]	cp_{NEF} [-]	cp_{WIN} [-]	$cp_{NEF}+cp_{WIN}$ [-]
Low-Speed	"+"	0.25	7.0	30	1.2	0.059	0.141	0.2
High-Speed	"∗"	0.8	4.5	0	0.6	0.187	0.013	0.2

(10) $$P_{T,0} = P_0 \cdot \left(1 + \frac{\gamma-1}{2} \cdot M_0^2\right)^{\frac{\gamma}{\gamma-1}} \quad .$$

Multiplication of both sides of Eq. (9) with $P_{T,0}/P_0$ yields

(11) $$FNPR = \frac{P_{T,0}}{P_0} \cdot FPR \quad .$$

The freestream pressure ratio may be substituted by the Mach number expression of Eq. (10). Hence, the FNPR can be calculated based on *FPR* and M_0.

Note that the delta in discharge coefficient is defined with opposite sign in the present study in comparison to [3] respectively Eq. (8)

(12) $$\Delta c_D = c_{D,FNPR} \cdot \left(\frac{\dot{m}_{FNPR}}{\dot{m}_{PR19}} - 1\right) = -\Delta c_{D,SAE} \quad .$$

If only the percentage change is considered, Eq. (12) can be divided by $c_{D,FNPR}$ and the expression in parentheses remains as the effective parameter.

Gross thrust for a single stream flow engine has already been defined by Eq. (1). In case of an air breathing engine moving relative to the ingested air, the net thrust is the difference between the nozzle gross thrust and the ram drag (compare also [2])

(13) $$F_N = F_G - F_E$$

while the ram drag is defined as

(14) $$F_E = \dot{m} \cdot V_0 \quad .$$

Inserting Eq.'s (1) and (14) into (13) and relating the biased net thrust in the numerator and the unbiased net thrust in the denominator and further subtracting 1, one obtains

(15) $$\left(\frac{F_{N,FNPR}}{F_{N,PR19}} - 1\right) = \frac{\dot{m}_{FNPR} \cdot (V_{100} - V_0)}{\dot{m}_{PR19} \cdot (V_{100} - V_0)} - 1 = \left(\frac{\dot{m}_{FNPR}}{\dot{m}_{PR19}} - 1\right) \quad .$$

Eq. (15) clearly shows that the relative bias error in net thrust is identical to the relative bias error in mass flow rate. This relation is obtained due to using the simple gross thrust definition based on the idea of the ideally fully expanded jet velocity $V_{100} = f(P_{T,19}, P_{100}, T_{T,19})$ far behind the engine. The errors incurred in comparison to the standard gross thrust definitions based on the nozzle exit flow velocity and an additional pressure term [3] are small and practically negligible for transonic transport aircraft applications.

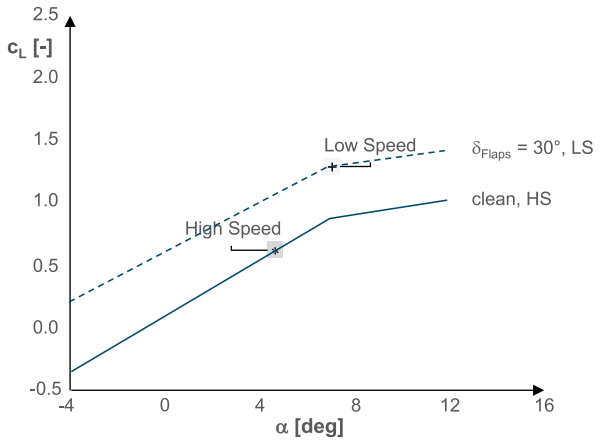

FIG 17. Lift curves for low speed take-off (LS) and high speed (HS) cruise operating points

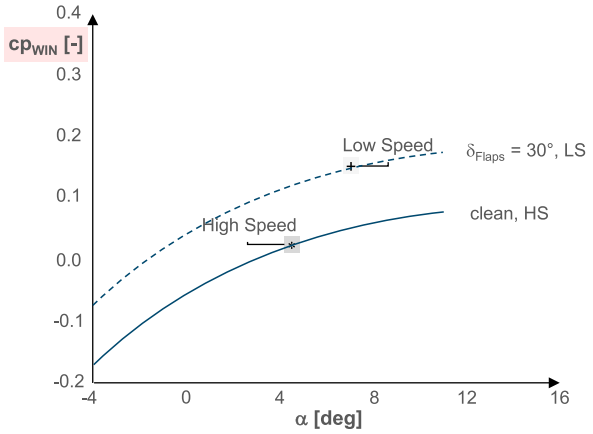

FIG 18. Wing induced fan nozzle cp's for low speed take-off (LS) and high speed (HS) operating points

In addition to the parametric evaluation of the introduced equations with FPR as parameter in FIG 19 and FIG 20, typical operating conditions in low- and high-speed operations are also shown based on the assessments made in chapters 2 and 3.

First, the NEF effect for low and high-speed conditions for a typical separate fan and core nozzle VHBR engine is depicted in FIG 15.

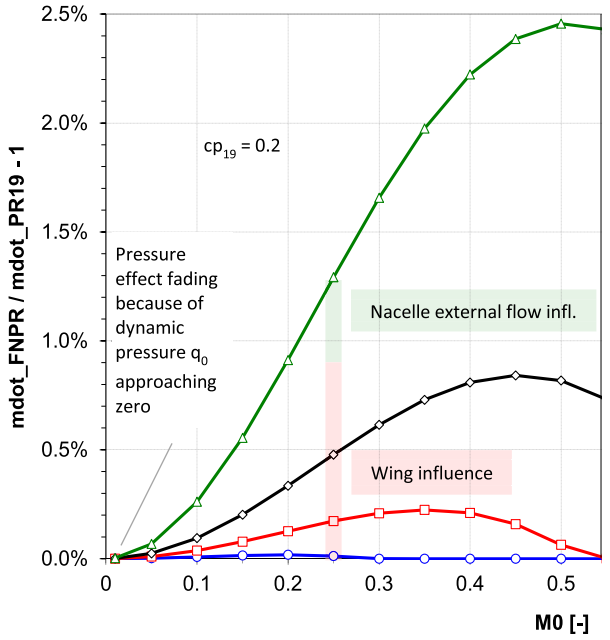

FIG 19. Low speed flow suppression in terms of discharge coefficient change

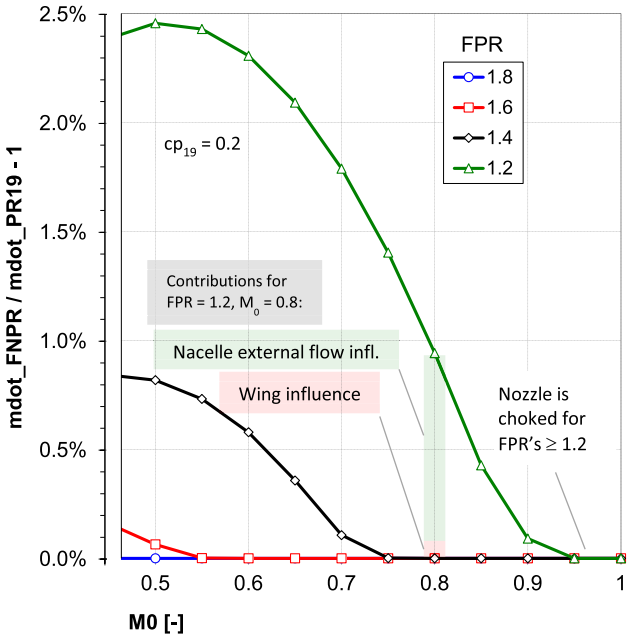

FIG 20. High speed flow suppression in terms of discharge coefficient change

Second, FIG 18 represents the wing induced WIN flow suppression at the nacelle nozzle exit stations while the operating points in terms of lift coefficients are illustrated in FIG 17.

TAB 2 summarizes the assumptions for both effects. For the subsequent analysis it is assumed valid to just arithmetically add both separate contributions. It can be shown that this is justifiable with little error particularly when both cp-contributions have the same sign and when the resulting cp is small which is the case for the chosen example combined value of 0.2.

For an *FPR = 1.8*, flow suppression is zero for Mach numbers of $M_0 = 0.3$ and greater because the fan nozzle is choked (FIG 19). For lower freestream Mach numbers, the bias effect on discharge coefficient and fan net trust is generally small. When the *FPR* decreases, fan nozzle choking is starting at higher Mach numbers. At an *FPR = 1.2* representative of future extreme high bypass ratio turbofan engine designs the fan nozzle is unchoked throughout the full Mach number operating range (FIG 20).

Regarding the magnitude of flow suppression bias, effects are greatest about half way between zero Mach and choking. The peak percentage bias in FIG 19 is 2.45% at $M_0 = 0.5$ for the lowest *FPR* of *1.2*.

For M_0 approaching zero, the flow suppression effect becomes always zero because the nozzle pressure P_{19} is approaching P_0 due to the constant $cp_{19} = 0.2$ model.

The red bars in the plots indicate the wing influence and the green bars that of external nacelle flow. Clearly, the wing influence dominates in low-speed conditions while the external nacelle flow effect is greater in magnitude in high-speed conditions. For the selected example with *FPR = 1.2*, the bias error is close to 1% and hence significant.

According to industry practice, only the NEF effects are corrected for in terms of engine thrust while the WIN influences are bookkept as aircraft drag.

This has the greatest impact in low speed flight where the WIN effects can be greater than the NEF effects. For future EHBR-type (Extreme High Bypass Ratio) turbofan engines with fan pressure ratios of 1.2, the WIN bias in low speed high lift take-off conditions can be as high as a percent of the mass flow rate. This translates into an equivalent net thrust error. Given that the thrust in the initial climb phase can be four times greater than the airframe drag, one percent error in thrust translates into four percent of drag error when the error is bookkept in terms of airframe drag. This is the same order of magnitude as drag due to the interference of the engine installation, the engine jets and the airframe in this configuration which is determined by means of powered wind tunnel tests with turbofan propulsion simulators ("jet effects") [12]. It is worth to recall that any overprediction of mass flow and thrust automatically yields an overprediction of derived airframe drag.

5. ENHANCED EXPERIMENTAL DATA REDUCTION APPROACH

Let's recall that the flow suppression bias errors in mass flow rates and net thrusts stem from the assumption of freestream static pressure (free flight & wind-tunnel: $P_{100} = P_{00} = P_0$) while the actual nozzle exit static pressure (fan: P_{19}, core: P_9) may be different. The biased "legacy" data reduction approach is illustrated by the measurement setup sketched in FIG 21 a).

Note that a set of data according to the compressible continuity Eq. (2) is required for all cases without

downstream choking.

This is

- *PT* Total Pressure
- *TT* Total Temperature
- *P* Static Pressure
- *A* Geometrical Nozzle/ Duct Cross Section Area

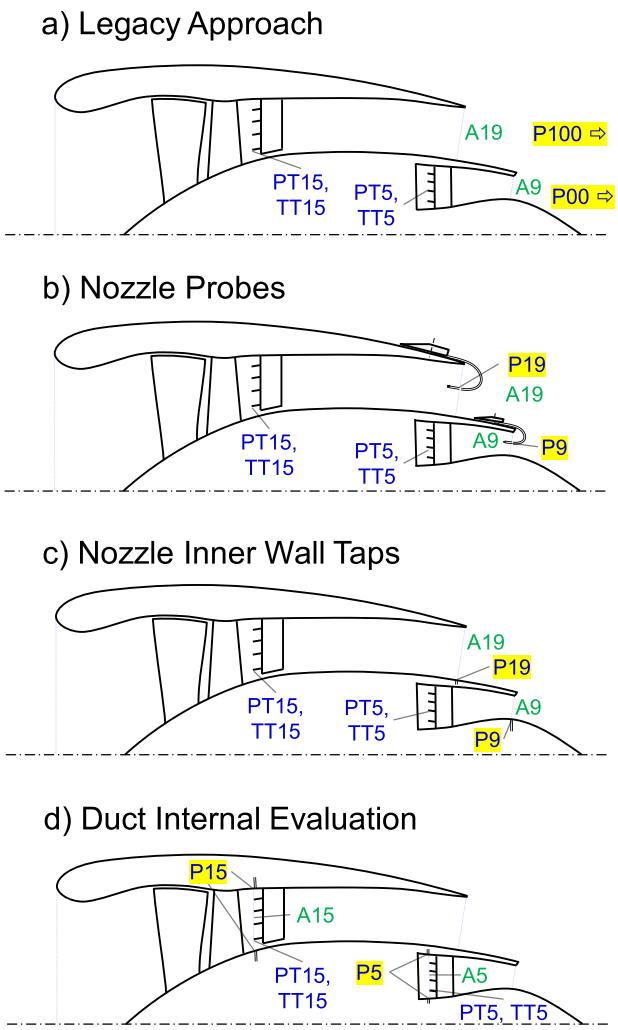

FIG 21. Turbofan instrumentation and data reduction approaches for mass flow rate determination based on gas path measurements

Because of no account for the nozzle, duct, and instrumentation losses a mass flow calibration is mandatory in any case as described in chapters 1 and 3.2.

An approach to generally avoid errors due to flow suppression is to base the data reduction on the actual static pressures at the evaluation station. Despite the fact that actual nozzle exit station pressures can be measured with static pressure probes (FIG 21, b)), this is not very practical for in-flight measurements because the probes would produce significant additional pressure and thrust losses.

Instead of immersive nozzle probes, wall static taps at the nozzle exit station could be used (FIG 21, c)). However, a challenge is that the probes on the inner wall may not be representative enough of the average pressure in the nozzle exit station as pointed out in [3].

An alternative is to move the mass flow rate evaluation station forward into the bypass duct (FIG 21, d)). This is possible because the continuity equation is valid at any station of a stream tube. Inside the duct, the static pressure can be conveniently measured with wall pressure taps. A convenient location may be the total pressure and total temperature measurement station inside the duct. For the mass flow rate determination, the local duct cross section area is required (instead of the nozzle exit area).

There may be local pressure distortions by the intrusive total pressure and temperature probes. Furthermore, utilizing standard instrumentation, the wall boundary layers are not resolved. Thus, a mass flow calibration is still required.

Measurements following this approach have already been successfully made for isolated and installed wind tunnel powered tests with Turbofan Propulsion Simulators (TPS). Comparison of the modified (“no suppression effects”) with the classical (“with suppression bias”) data reduction approach made it possible to quantify the bias effects. The match with CFD simulations comparable to those described in the present paper was good.

6. SUMMARY AND OUTLOOK

Sensitivities of engine fan and core mass flow rate computation to the static pressure at the nozzles and also the assumptions for data reduction have been shown. Aircraft with their engines mounted under the wing are particularly affected.

The present study is mainly based on RANS results. Only the flap effect was retained from the previous VLM-based study.

For the airframe (respectively wing or WIN) influences, the trailing edge flap effect is greatest followed by the angle of attack, the freestream Mach number, nozzle geometry and sideslip angle effects. The NEF effect can have the greatest influence with particularly high nozzle pressures for through flow nacelles.

According to industry practice, only the NEF effects are corrected for in terms of engine thrust while the WIN influences are bookkept as aircraft drag.

This has the greatest impact in low speed flight where the WIN effects can be greater than the NEF effects. For future EHBR-type turbofan engines with fan pressure ratios of 1.2, the WIN bias in low speed high-lift take-off conditions can be as high as one percent of the mass flow rate. This translates into an equivalent net thrust bias error. Without tackling the bias effect by either an appropriate measurement and data reduction approach or a correction, the resulting bias error in drag is up to four times the mass flow error.

In order to avoid systematic errors due to nozzle backpressure effects, the local static pressures are required for experimental data reduction in wind tunnel and flight testing. A straight forward approach based on the conservation of mass, is to move the evaluation station from the nozzle exit station to a duct internal station where it is more convenient to measure static pressures than at the nozzle exit stations.

In order to reduce uncertainties due to synthesis of data from different sources obtained with different CFD methods, it would be desirable to complement the RANS study based on the HS-CRM with TFN's by

- simulations of the LS-CRM in high lift take off configuration
- simulations with powered nacelles.

Particularly the latter would help drawing a more realistic picture compared to the peculiar HS-CRM through flow nacelles with their particularly high nozzle pressure coefficients.

ACKNOWLEDGEMENTS

The research presented in this publication has been conducted by the Research Group for Aircraft Systems of TU Wien. The Research Group receives funding from the Austrian Aviation Programme TAKE OFF via the BMK Endowed Professorship for Innovative Aviation Technologies.

Contact address:

martin.berens@tuwien.ac.at

REFERENCES

[1] de Wolf, B. W. (1996). Possibilities and Limitations of VHBR and UHBR Turbofan Simulations in Engine/Airframe Integration Wind Tunnel Experiments. pp. 15-21, In 'Aspects of Engine-Airframe Integration for Transport Aircraft. Proceedings of the DNW Workshop Braunschweig' (Ed. Hoheisel, H.), DLR-Mitteilung 96-01.

[2] Guide to In-Flight Thrust Measurement of Turbojets and Fan Engines. (1979). AGARD-AG-237.

[3] In-Flight Thrust Determination. (2017). SAE AIR 1703. Rev. A. Society of Automotive Engineers. USA.

[4] Vassberg, John C., DeHaan, Mark, A., Rivers, Melissa S. & Wahls, Richard A. (2008). Development of a Common Research Model for Applied CFD Validation Studies. AIAA-2008-6919.

[5] Rivers, M., Quest, J., Rudnik, R., (2015). Comparison of the NASA Common Research Model European Transonic Wind Tunnel Test Data to NASA Test Data. AIAA SciTech Forum. 53rd AIAA Aerospace Sciences Meeting, 5-9 January 2015, Kissimmee, Florida. AIAA-2015-1093.

[6] Lacy, Doug S. & Sclafani, Anthony J. (2016). Development of the High Lift Common Research Model (HL-CRM): A Representative High Lift Configuration for Transonic Transports. 54th AIAA Aerospace Sciences Meeting, 4-8 January 2016, San Diego, AIAA 2016-0308.

[7] Berens, M., de Rosa Jacinto da Silva, M. (2022). Airframe induced flow suppression effects on turbofan engines. 56th 3AF International Conference on Applied Aerodynamics 28 – 30 March 2022, Toulouse – France.

[8] Berens, M. (2008). Potential of Multi-Winglet Systems to Improve Aircraft Performance, PhD thesis Technische Universität Berlin. DOI: 10.14279/depositonce-1916.

[9] Hartwich, Peter M., et.al. (2016). Refined AFC-Enabled High-Lift System Integration Study. NASA/CR-2016-219170.

[10] Torenbeek, Egbert. (1982). Synthesis of Subsonic Airplane Design. Delft University Press. p. 530.

[11] Sabater Campomanes, Christian. (2017). External Flow Effects in the Engine/Airframe Integration Technique – A new Thrust/Drag Bookkeeping Approach at the German-Dutch Wind Tunnels. Master Thesis TU Delft. http://resolver.tudelft.nl/uuid:e9e66768-b0be-49f0-970a-1a9adf41a377.

[12] Hünecke, K. (2004). Die Technik des modernen Verkehrsflugzeuges. 3rd ed. Motorbuch Verlag. Stuttgart.